Supplementary information

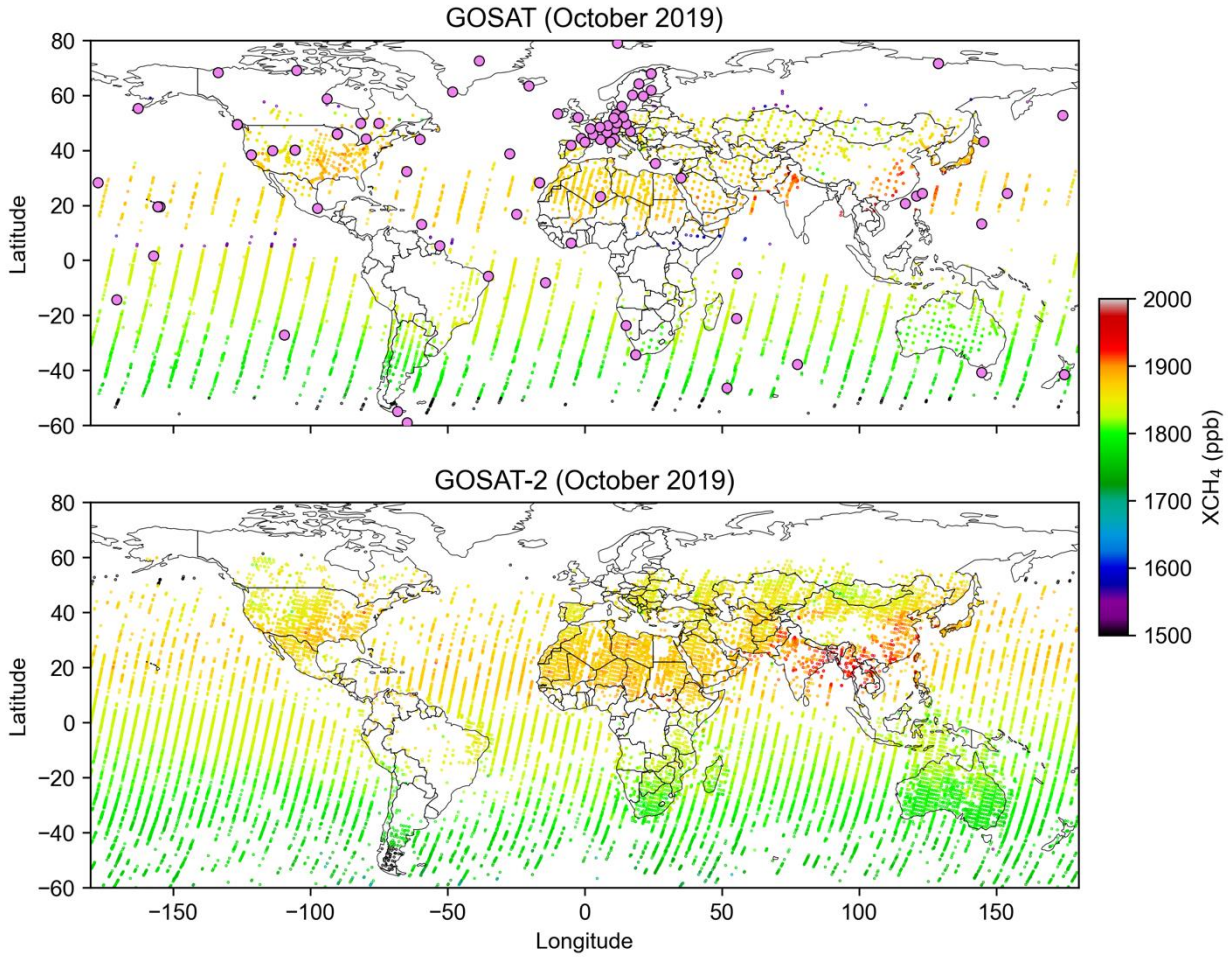


Figure S1. GOSAT and GOSAT-2 XCH_4 observations for the month of October 2019 along with surface observation sites used in inversion (violet circles in the upper panel).

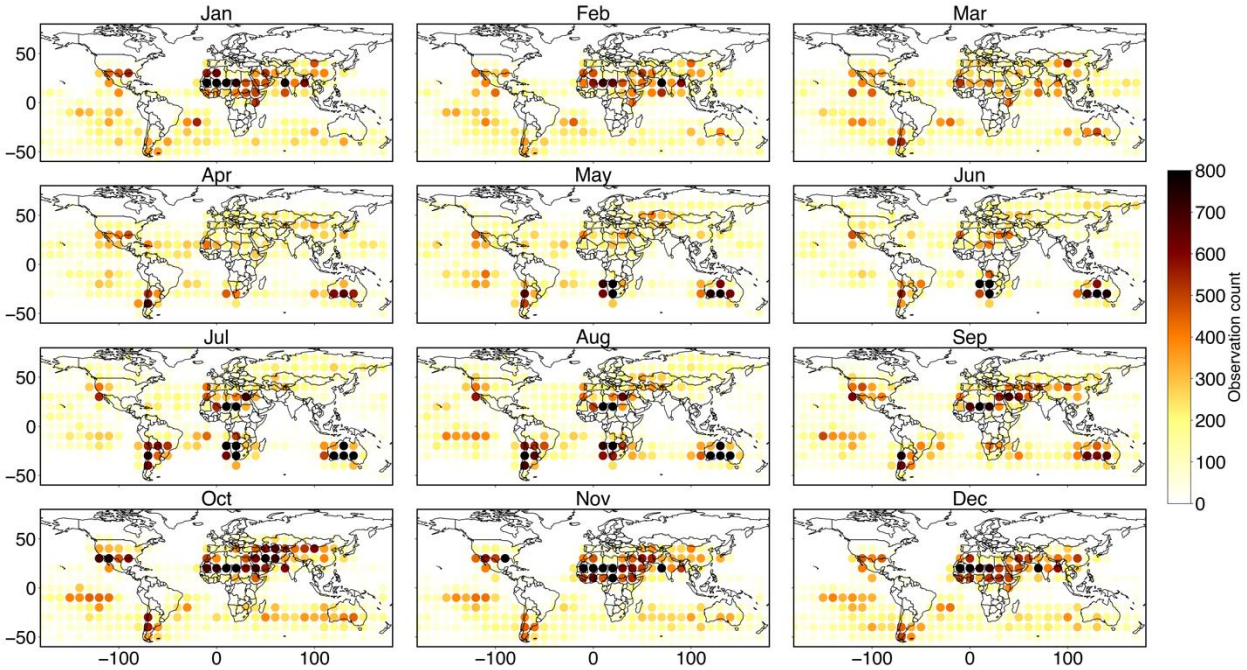


Figure S2. Number of GOSAT observations in 10°×10° grids for the 2019-2022 period for each month.

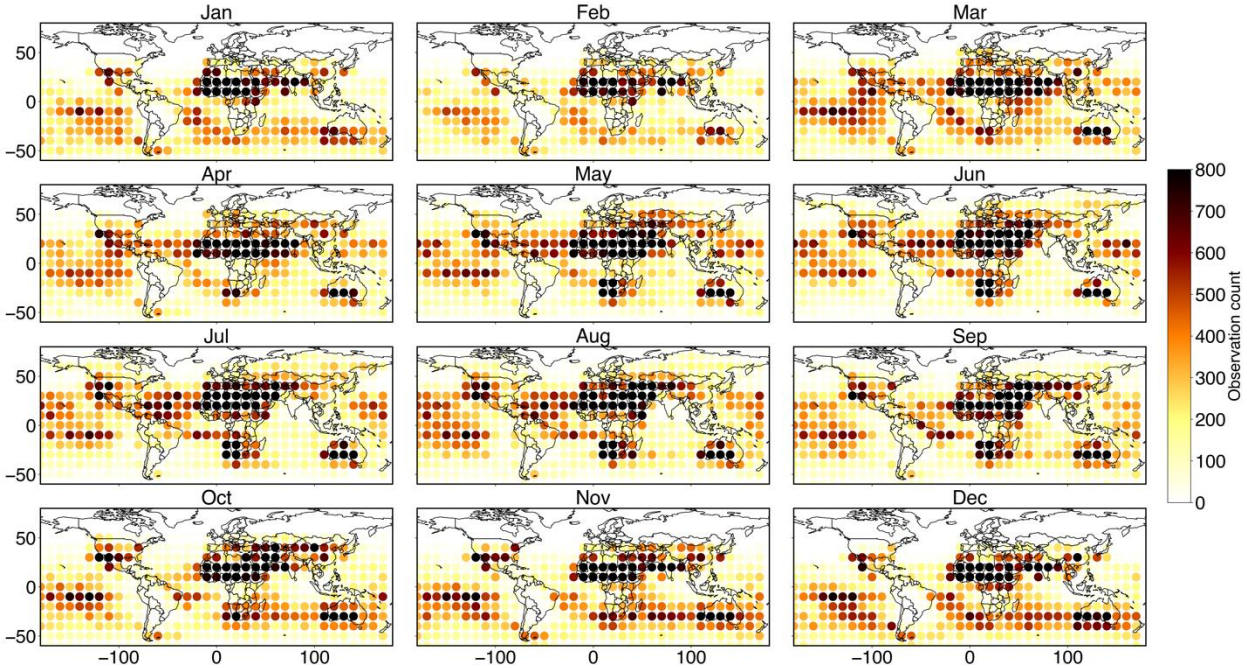


Figure S3. Number of GOSAT-2 observations in 10°×10° grids for the 2019-2022 period for each month.

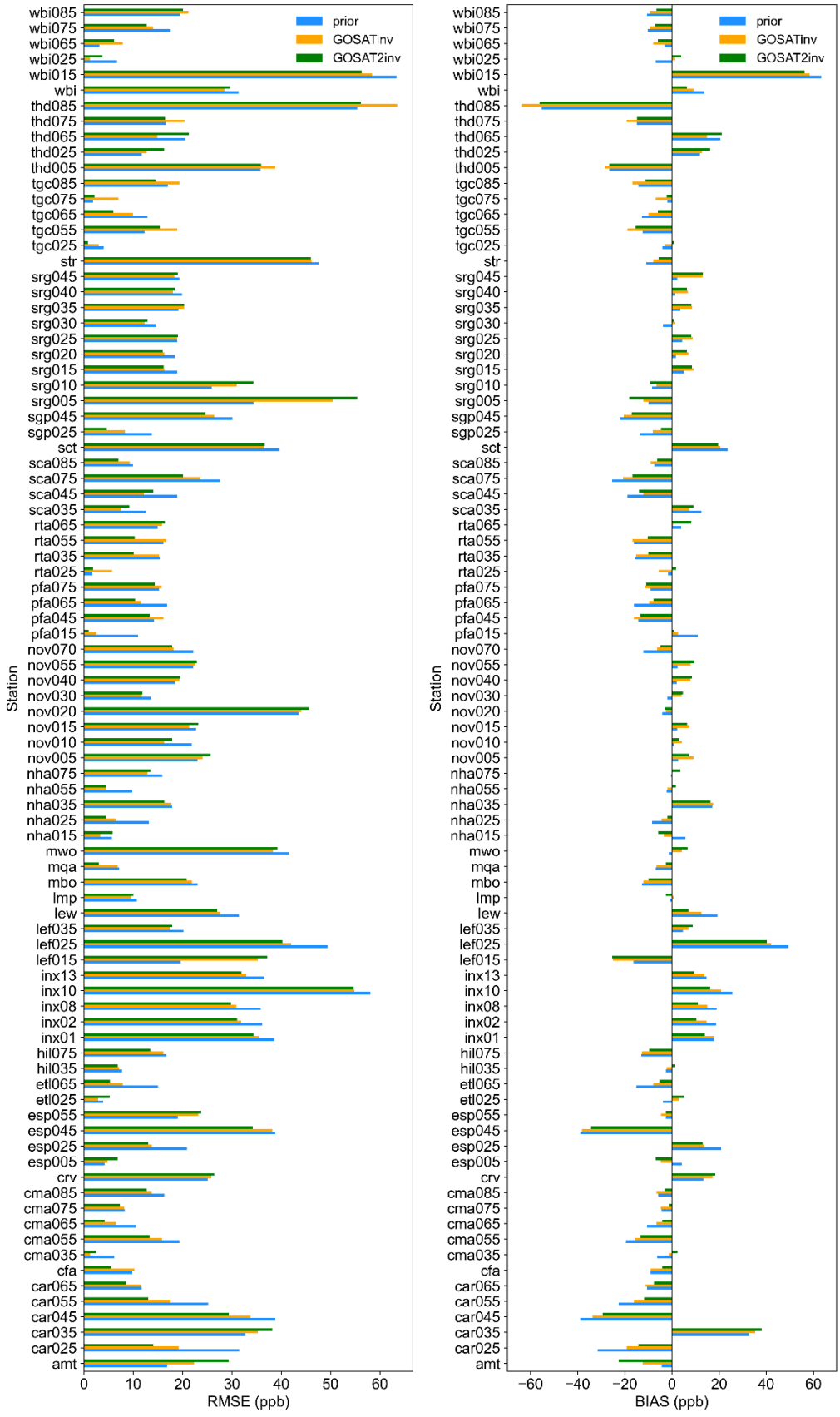

prior
GOSATinv
GOSAT2inv
Station
RMSE (ppb)
BIAS (ppb)
wbi085
wbi075
wbi065
wbi025
wbi015
wbi
thd085
thd075
thd065
thd025
thd005
tgc085
tgc075
tgc065
tgc055
tgc025
str
srg045
srg040
srg035
srg030
srg025
srg020
srg015
srg010
srg005
sgp045
sgp025
sct
sca085
sca075
sca045
sca035
rta065
rta055
rta035
rta025
pfa075
pfa065
pfa045
pfa015
nov070
nov055
nov040
nov030
nov020
nov015
nov010
nov005
nha075
nha055
nha035
nha025
nha015
mwo
mqa
mbo
lmp
lew
lef035
lef025
lef015
inx13
inx10
inx08
inx02
inx01
hil075
hil035
etl065
etl025
esp055
esp045
esp025
esp005
crv
cma085
cma075
cma065
cma055
cma035
cfa
car065
car055
car045
car035
car025
amt
0
10
20
30
40
50
60
−60
−40
−20
0
20
40
60

Figure S4. RMSE and BIAS for prior and optimized forward simulations for GOSAT and GOSAT-2 for the validation sites. The site codes with three-digit extensions are for aircraft data, with the site code showing the station code with the altitude bin appended in units of hundred meters. Site codes with two digits show the tower with digits showing height in units of ten meters.

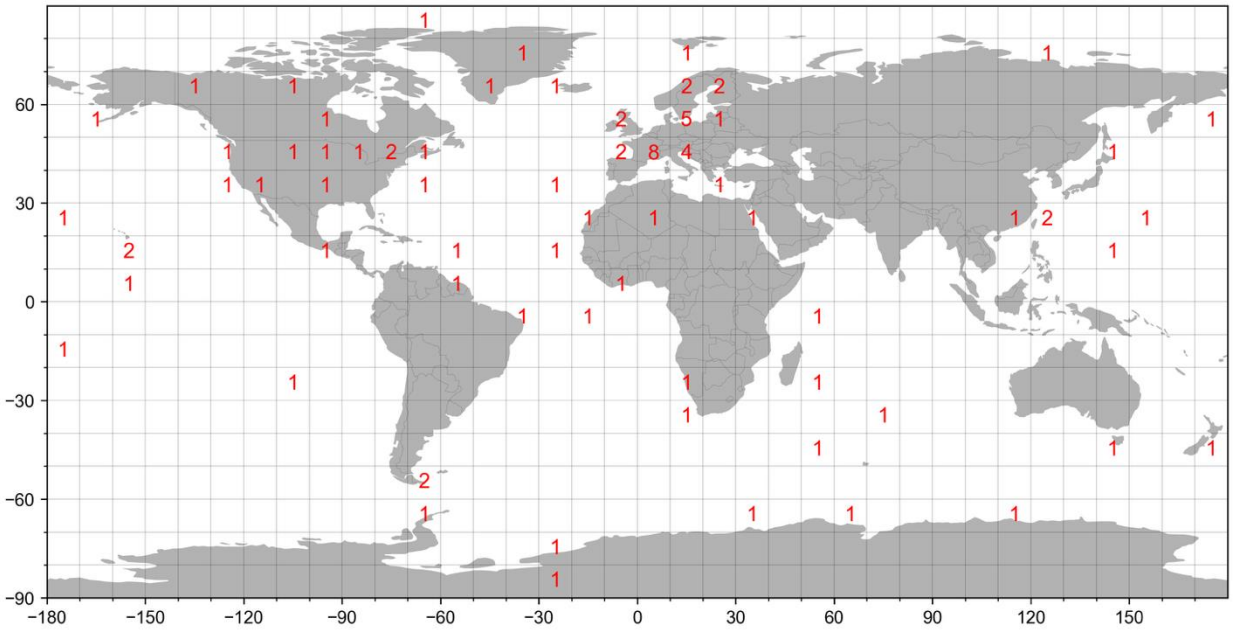


Figure S5. The number of surface observation sites in each 10°×10° grids to show the spatial representativeness of observation sites. A large part of Asia, Africa, Australia, and South America is not covered by surface observation stations.

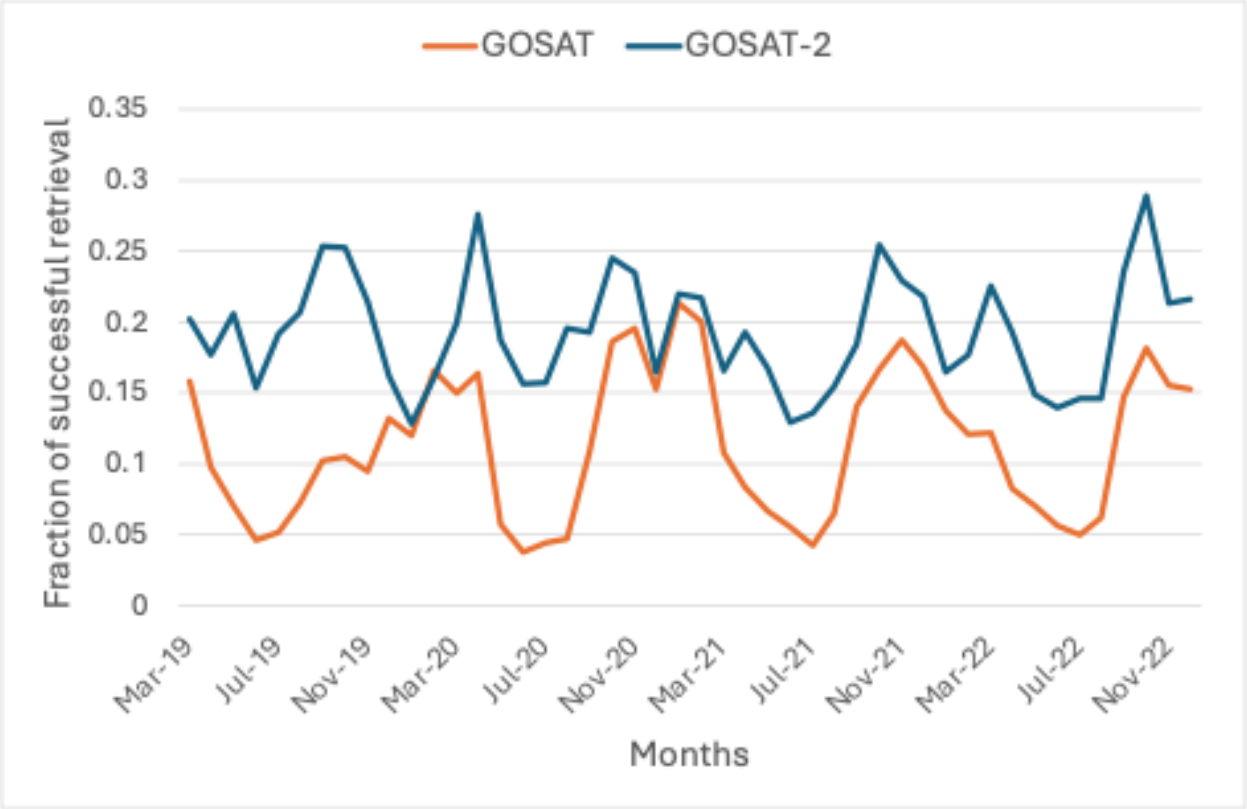


Figure S6. Monthly fraction (defined as total XCH_4 retrievals/ total observations) of successful retrievals for GOSAT and GOSAT-2 over East Asia (80-125E; 20-55N) for the analysis period.

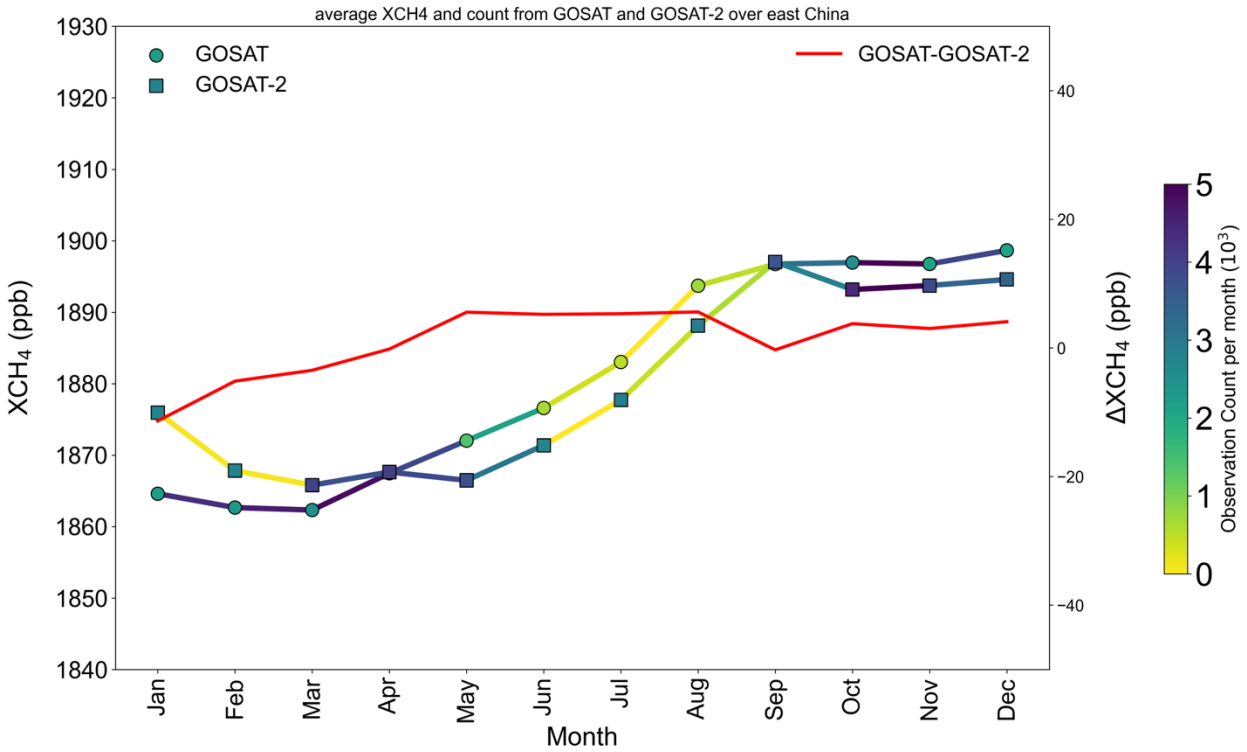


Figure S7. The monthly climatological mean of the XCH_4 field from GOSAT and GOSAT-2 over the east asian domain (100-135E; 15-50N) showing the mean difference between the products. The colors indicate the observations count in thousands per month for GOSAT and GOSAT-2. The difference (GOSAT-GOSAT-2) of XCH_4 is also shown.

Estimating the effect of seasonal sampling bias between GOSAT and GOSAT-2

In order to calculate the BIAS due to sampling differences (lower data count for GOSAT during the cloudy season), we randomly subsampled the GOSAT-2 XCH_4 data to match the data count to that of GOSAT in a month. We selected a region (SE Asia) that is tropical and prone to seasonal sampling biases. The area mean of the sub-sampled GOSAT-2 data approximates the loss of cloud screening in GOSAT data. So the difference between the mean of total GOSAT-2 and sub-sampled GOSAT-2 over the selected region provides approximately the bias in GOSAT due to seasonal sampling biases. We apply this bias in a regression equation relating the monthly difference in GOSAT and GOSAT-2 XCH_4 (ΔXCH_4) and the corresponding posterior total flux difference (ΔFlux) in inversion. The regression was weighted by uncertainty both in ΔXCH_4 and ΔFlux. We take this regression fit as a measure of inversion sensitivity to XCH_4 changes duw to lower successful retrievals in GOSAT during cloudy season. By converting the ΔXCH_4 to flux we arrive at approximately 7.3 Tg/year change in posterior total in this region.

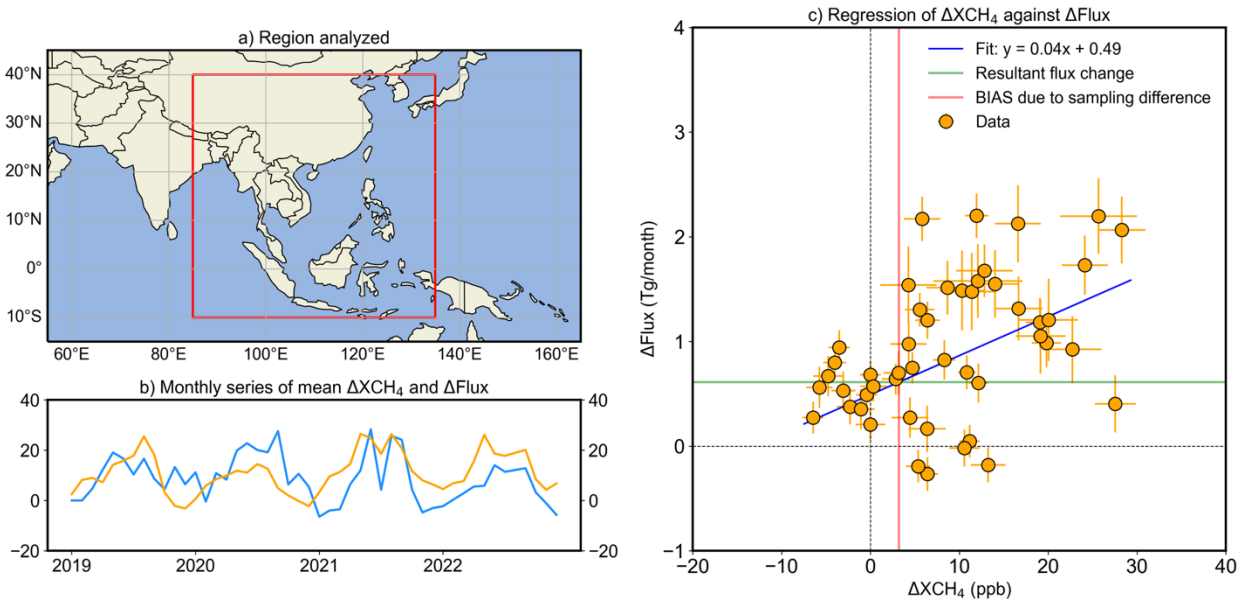


Figure S8. A) The region marked by the red rectangle shows the analysis region. B) monthly time series of ΔXCH_4 and ΔFlux over the marked region. C) regression of ΔXCH_4 and ΔFlux. The red line shows the mean bias over this region due to sampling biases in GOSAT, green line shows the corresponding flux change in Tg/month

Table S1. Details of surface/ship/aircraft observations used in this study.

Site	Name	Latitude	Longitude	Sampling type	Lab	References
ALT	Alert, Nunavut	82.45	-62.51	surface-flask	NOAA, CSIRO	(Lan et al., 2024)
ALT	Alert, Nunavut	82.45	−62.51	surface-in situ	ECCC	(Worthy et al., 2003)
AMS	Amsterdam Island	−37.80	77.54	surface-flask	NOAA	(Lan et al., 2024)
AOA	Aircraft Observation of Atmospheric trace gases by JMA			aircraft-flask	JMA	(Schuldt et al., 2021) 8/23/2025 5:26:00 PM
ASC	Ascension Island	−7.97	−14.40	surface-flask	NOAA	(Lan et al., 2024)
ASK	Assekrem	23.26	5.63	surface-flask	NOAA	(Lan et al., 2024)
AZR	Terceira Island, Azores	38.77	−27.38	surface-flask	NOAA	(Lan et al., 2024)
BHD	Baring Head Station	−41.41	174.87	surface-flask	NOAA	(Lan et al., 2024)
BHD	Baring Head Station	−41.41	174.87	surface-in situ	NIWA	(Lowe et al., 1991)
BIS	Biscarrosse	44.38	−1.23	surface-in situ	LSCE	(Lopez and Ramonet, 2024)
BMW	Tudor Hill, Bermuda	32.26	−64.88	surface-flask	NOAA	(Lan et al., 2024)
CBA	Cold Bay, Alaska	55.21	−162.72	surface-flask	NOAA	(Lan et al., 2024)
CBY	Cambridge Bay, Nunavut Territory	69.13	−105.06	surface-in situ	ECCC	(Worthy et al., 2003)
CGO	Cape Grim, Tasmania	−40.68	144.69	surface-flask	NOAA	(Lan et al., 2024)
CHL	Churchill, Manitoba	58.74	−93.82	surface-in situ	ECCC	(Worthy et al., 2003)
CHR	Christmas Island	1.70	−157.15	surface-flask	NOAA	(Lan et al., 2024)

CIB	Centro de Investigacion de la Baja Atmosfera (CIBA)	41.81	−4.93	surface-flask	NOAA	(Lan et al., 2024)
CMN	Mt. Cimone Station	44.19	10.70	surface-in situ	UNIURB, ICOS-ATC, CNR-ISAC	(Cristofanelli and Trisolino, 2020)
CON	CONTRAIL (Comprehensive Observation Network for TRace gases by AIrLiner)			aircraft-flask	NIES, MRI	(Machida et al., 2008)
CPS	Chapais, Quebec	49.82	−74.98	surface-in situ	ECCC	(Worthy et al., 2003)
CPT	Cape Point	−34.35	18.49	surface-flask	NOAA	(Lan et al., 2024)
CPT	Cape Point	−34.35	18.49	surface-in situ	SAWS	(Schuldt et al., 2021) 8/23/2025 5:26:00 PM
CRZ	Crozet Island	−46.43	51.85	surface-flask	NOAA	(Lan et al., 2024)
CVO	Cape Verde Observatory	16.86	−24.87	surface-in situ	CEDA, MPI-BGC	(Kozlova, 2020)
CYA	Casey, Antarctica	−66.28	110.52	surface-flask	CSIRO	(Etheridge et al., 2021)
DRP	Drake Passage			shipboard-flask	NOAA	(Schuldt et al., 2021) 8/23/2025 5:26:00 PM
DSI	Dongsha Island	20.70	116.73	surface-flask	NOAA	(Lan et al., 2024)
EGB	Egbert, Ontario	44.23	−79.78	surface-in situ	ECCC	(Worthy et al., 2003)
EIC	Easter Island	−27.16	−109.43	surface-flask	NOAA	(Lan et al., 2024)
ERS	Ersa	42.97	9.38	surface-in situ	LSCE	(Delmotte et al., 2025a)
ESP	Estevan Point, British Columbia	49.38	−126.54	surface-flask	CSIRO	(Schuldt et al., 2021) 8/23/2025 5:26:00 PM
ESP	Estevan Point, British Columbia	49.38	−126.54	surface-in situ	ECCC	(Worthy et al., 2003)
FKL	Finokalia	35.34	25.67	surface-in situ	ECPL	(Delmotte et al., 2025b)
FSD	Fraserdale	49.88	−81.57	surface-in situ	ECCC	(Worthy et al., 2003)
GAT	Gartow	53.07	11.44	surface-in situ	ICOS-ATC, HPB	(ICOS RI, 2021; Kubistin et al., 2025a)
GMI	Mariana Islands	13.39	144.66	surface-flask	NOAA	(Lan et al., 2024)
GUY	GuyaFlux	5.28	−52.91	surface-in situ	EcoFoG	
HAT	Hateruma	43.16	145.50	surface-in situ	NIES	(Tohjima et al., 2002)
HBA	Halley Station, Antarctica	−75.61	−26.21	surface-flask	NOAA	(Lan et al., 2024)
HPB	Hohenpeissenberg	47.80	11.02	surface-flask	NOAA	(Lan et al., 2024)
HPB	Hohenpeissenberg	47.80	11.02	surface-in situ	ICOS-ATC, HPB	(ICOS RI, 2021; Kubistin et al., 2025b)
HTM	Hyltemossa	56.10	13.42	surface-in situ	ICOS-ATC, LUND-CEC	(Heliasz and Biermann, 2025; ICOS RI, 2021)
HUN	Hegyhátsál	46.95	16.65	surface-flask	NOAA	(Lan et al., 2024)
IAGOS	In-service Aircraft for a Global Observing System			aircraft-flask	KIT/IMK-ASF, IAU	(Schuldt et al., 2021) 8/23/2025 5:26:00 PM
IAGOS	In-service Aircraft for a Global Observing System			aircraft-in situ	KIT/IMK-ASF, MPI-BGC	(Schuldt et al., 2021) 8/23/2025 5:26:00 PM
ICE	Storhofdi, Vestmannaeyjar	63.40	−20.29	surface-flask	NOAA	(Lan et al., 2024)
INU	Inuvik, Northwest Territories	68.32	−133.53	surface-in situ	ECCC	(Worthy et al., 2003)
IVI	Ivittuut	61.21	−48.17	surface-in situ	LSCE	(Delmotte and Ramonet, 2025)

IZO	Izana, Tenerife, Canary Islands	28.31	−16.50	surface-flask	NOAA	(Lan et al., 2024)
IZO	Izana, Tenerife, Canary Islands	28.31	−16.50	surface-in situ	AEMET	(Gomez-Pelaez et al., 2006)
JFJ	Jungfraujoch	46.55	7.99	surface-in situ	ICOS-ATC, HFSJG, EMPA	(Emmenegger et al., 2025; ICOS RI, 2021)
KIT	Karlsruhe	49.09	8.42	surface-in situ	ICOS-ATC, HPB	(ICOS RI, 2021; Kubistin et al., 2025c)
KRE	Kresin u Pacova	49.58	15.08	surface-in situ	ICOS, CAS	(ICOS RI, 2021; Marek et al., 2025)
KUM	Cape Kumukahi, Hawaii	19.56	−154.89	surface-flask	NOAA	(Lan et al., 2024)
LEF	Park Falls, Wisconsin	45.95	−90.27	surface-flask	NOAA	(Lan et al., 2024)
LEF	Park Falls, Wisconsin	45.95	−90.27	surface-pfp	NOAA, UofWI	(Schuldt et al., 2021) 8/23/2025 5:26:00 PM
LEF	Park Falls, Wisconsin	45.95	−90.27	tower-in situ	NOAA, UofWI	(Andrews et al., 2014)
LIN	Lindenberg	52.17	14.12	surface-in situ	ICOS-ATC, HPB	(ICOS RI, 2021; Kubistin et al., 2025d)
LLN	Lulin	23.47	120.87	surface-flask	NOAA	(Lan et al., 2024)
LTO	Lamto	6.22	−5.03	surface-in situ	LSCE	(Tiemoko et al., 2021)
MAA	Mawson Station, Antarctica	−67.62	62.87	surface-flask	CSIRO	(Schuldt et al., 2021) 8/23/2025 5:26:00 PM
MEX	High Altitude Global Climate Observation Center	18.98	−97.31	surface-flask	NOAA	(Lan et al., 2024)
MHD	Mace Head, County Galway	53.33	−9.90	surface-flask	NOAA	(Lan et al., 2024)
MID	Sand Island, Midway	28.22	−177.37	surface-flask	NOAA	(Lan et al., 2024)
MLO	Mauna Loa, Hawaii	19.54	−155.58	surface-flask	NOAA, CSIRO	(Lan et al., 2024; Schuldt et al., 2021)
MLO	Mauna Loa, Hawaii	19.54	−155.58	surface-in situ	NOAA	(Dlugokencky et al., 1995)
MNM	Minamitorishima	24.28	153.98	surface-in situ	JMA	(Schuldt et al., 2021) 8/23/2025 5:26:00 PM
NAT	Farol De Mae Luiza Lighthouse	−5.80	−35.19	surface-flask	NOAA	(Lan et al., 2024)
NMB	Gobabeb	−23.58	15.03	surface-flask	NOAA	(Lan et al., 2024)
NOR	Norunda	60.09	17.48	surface-in situ	ICOS-ATC, LUND-CEC	(ICOS RI, 2021; Lehner, 2025)
NWR	Niwot Ridge, Colorado	40.05	−105.59	surface-flask	NOAA	(Lan et al., 2024)
NWR	Niwot Ridge, Colorado	40.05	−105.59	surface-pfp	NOAA	(Schuldt et al., 2021) 8/23/2025 5:26:00 PM
OHP	Observatoire de Haute Provence	43.93	5.71	surface-in situ	OSU	(Blanc et al., 2025)
OPE	Observatoire perenne de l'environnement	48.56	5.50	surface-in situ	ICOS-ATC, LSCE	(ICOS RI, 2021; Ramonet et al., 2025a)
OXK	Ochsenkopf	50.03	11.81	surface-flask	NOAA	(Lan et al., 2024)
OXK	Ochsenkopf	50.03	11.81	surface-in situ	ICOS-ATC, HPB	(ICOS RI, 2021; Kubistin et al., 2025e)
PAL	Pallas-Sammaltunturi, GAW Station	67.97	24.12	surface-flask	NOAA	(Lan et al., 2024)
PAL	Pallas-Sammaltunturi, GAW Station	67.97	24.12	surface-in situ	ICOS-ATC, FMI	(Hatakka, 2025; ICOS RI, 2021)
PDM	Pic du Midi	42.94	0.14	surface-in situ	LSCE	(ICOS RI, 2021)

POC	Pacific Ocean			shipboard-flask	NOAA	(Lan et al., 2024)
PSA	Palmer Station, Antarctica	−64.77	−64.05	surface-flask	NOAA	(Lan et al., 2024)
PUY	Puy de Dome	45.77	2.97	surface-in situ	ICOS-ATC, LSCE	(Colomb et al., 2025)
RGL	Ridge Hill	52.00	−2.54	tower-in situ	UNIVBRIS	(Stanley et al., 2025)
RPB	Ragged Point	13.17	−59.43	surface-flask	NOAA	(Lan et al., 2024)
RUN	La Réunion	−21.08	55.38	surface-in situ	ICOS-ATC, LSCE	(De Mazière et al., 2025)
SEY	Mahe Island	−4.68	55.53	surface-flask	NOAA	(Lan et al., 2024)
SGP	Southern Great Plains, Oklahoma	36.61	−97.49	surface-in situ	LBNL-ARM	(Schuldt et al., 2021) 8/23/2025 5:26:00 PM
SHM	Shemya Island, Alaska	52.71	174.13	surface-flask	NOAA	(Lan et al., 2024)
SMO	Tutuila	−14.25	−170.56	surface-flask	NOAA	(Lan et al., 2024)
SMR	Hyytiala	61.85	24.29	surface-in situ	ICOS-ATC, UHELS	(ICOS RI, 2021; Mammarella, 2025)
SPO	South Pole, Antarctica	−89.98	−24.80	surface-flask	NOAA, CSIRO	(Lan et al., 2024)
SUM	Summit	72.60	−38.42	surface-flask	NOAA	(Lan et al., 2024)
SVB	Svartberget	64.26	19.78	surface-in situ	ICOS-ATC, SLU	(ICOS RI, 2021; Larmanou and Marklund, 2025)
SYO	Syowa Station, Antarctica	−69.01	39.59	surface-flask	NOAA	(Lan et al., 2024)
SYO	Syowa Station, Antarctica	−69.01	39.59	surface-in situ	TU	(Aoki et al., 1992)
TIK	Hydrometeorological Observatory of Tiksi	71.60	128.89	surface-flask	NOAA	(Lan et al., 2024)
TIK	Hydrometeorological Observatory of Tiksi	71.60	128.89	surface-in situ	FMI, MGO	(Schuldt et al., 2021) 8/23/2025 5:26:00 PM
TOH	Torfhaus	51.81	10.54	surface-in situ	ICOS-ATC, HPB	(ICOS RI, 2021; Kubistin et al., 2025f)8/23/2025 5:26:00 PM
TRN	Trainou	47.96	2.11	surface-in situ	ICOS-ATC, LSCE	(ICOS RI, 2021; Ramonet et al., 2025b)
USH	Ushuaia	−54.85	−68.31	surface-flask	NOAA	(Lan et al., 2024)
UTA	Wendover, Utah	39.90	−113.72	surface-flask	NOAA	(Lan et al., 2024)
UTO	Uto	59.78	21.37	surface-in situ	ICOS-ATC, FMI	(Hatakka and Laurila, 2025; ICOS RI, 2021)
WGC	Walnut Grove, California	38.27	−121.49	surface-pfp	NOAA, LBNL	(Andrews et al., 2017)
WGC	Walnut Grove, California	38.27	−121.49	tower-in situ	NOAA, LBNL	(Andrews et al., 2014)
WIS	Weizmann Institute of Science at the Arava Institute, Ketura	29.96	35.06	surface-flask	NOAA	(Lan et al., 2024)
WSA	Sable Island, Nova Scotia	43.93	−60.01	surface-in situ	ECCC	(Worthy et al., 2003)
YON	Yonagunijima	24.47	123.02	surface-in situ	JMA	(Tsutsumi et al., 2006)
ZEP	Zeppelin	78.91	11.89	surface-flask	NOAA, ICOS-ATC, NILU	(ICOS RI, 2021; L. Myhre et al., 2021; Lan et al., 2024)

Table S2. Details of the observations used for validation of inversion.

Site	Name	Latitude	Longitude	Sampling type	Lab	References
AMT	Argyle, Maine	45.03	−68.68	surface-flask	NOAA	(Lan et al., 2024)
AMT	Argyle, Maine	45.03	−68.68	surface-pfp	NOAA	(Schuldt et al., 2021) 8/23/2025 5:26:00 PM
CAR	Briggsdale, Colorado			aircraft-pfp	NOAA	(McKain, 2024)
CFA	Cape Ferguson, Queensland	−19.28	147.06	surface-flask	CSIRO	(Schuldt et al., 2021)8/23/2025 5:26:00 PM
CMA	Offshore Cape May, New Jersey			aircraft-pfp	NOAA	(McKain, 2024)
CRV	Carbon in Arctic Reservoirs Vulnerability Experiment (CARVE)			aircraft-pfp	NOAA	(Sweeney et al., 2016)
CRV	Carbon in Arctic Reservoirs Vulnerability Experiment (CARVE)	64.99	−147.60	surface-pfp	NOAA	(Andrews A. et al., 2024)
CRV	Carbon in Arctic Reservoirs Vulnerability Experiment (CARVE)	64.99	−147.60	tower-in situ	NOAA	(Andrews A. et al., 2024)
ESP	Estevan Point, British Columbia			aircraft-pfp	NOAA	(McKain, 2024)
ETL	East Trout Lake, Saskatchewan			aircraft-pfp	NOAA	(McKain, 2024)
ETL	East Trout Lake, Saskatchewan	54.35	−104.99	surface-in situ	ECCC	(Schuldt et al., 2021) 8/23/2025 5:26:00 PM
HIL	Homer, Illinois			aircraft-pfp	NOAA	(McKain, 2024; Sweeney et al., 2015)
INX	INFLUX (Indianapolis Flux Experiment)	39.58	-86.42	surface-pfp	NOAA	(Andrews et al., 2023)
LEF	Park Falls, Wisconsin			aircraft-pfp	NOAA	(McKain, 2024)
LEW	Lewisburg, Pennsylvania	40.94	−76.88	surface-pfp	NOAA	(Schuldt et al., 2021) 8/23/2025 5:26:00 PM
LMP	Lampedusa	35.52	12.63	surface-flask	NOAA	(Lan et al., 2024)
LMP	Lampedusa	35.52	12.63	surface-in situ	ICOS-ATC, ENEA	(Di Sarra et al., 2021; ICOS RI, 2021)
MBO	Mt. Bachelor Observatory	43.98	−121.69	surface-pfp	NOAA	(Schuldt et al., 2021) 8/23/2025 5:26:00 PM
MQA	Macquarie Island	−54.48	158.97	surface-flask	CSIRO	(Schuldt et al., 2021) 8/23/2025 5:26:00 PM
MWO	Mt. Wilson Observatory	34.22	−118.06	surface-pfp	NOAA	(Schuldt et al., 2021) 8/23/2025 5:26:00 PM
NHA	Offshore Portsmouth, New Hampshire (Isles of Shoals)			aircraft-pfp	NOAA	(McKain, 2024)
PFA	Poker Flat, Alaska			aircraft-pfp	NOAA	(McKain, 2024)
RTA	Rarotonga			aircraft-pfp	NOAA	(McKain, 2024)
SCA	Offshore Charleston, South Carolina			aircraft-pfp	NOAA	(McKain, 2024)
SCT	Beech Island, South Carolina	33.41	−81.83	surface-pfp	NOAA, SRNL	(Schuldt et al., 2021) 8/23/2025 5:26:00 PM
SCT	Beech Island, South Carolina	33.41	−81.83	tower-in situ	NOAA, SRNL	(Andrews et al., 2014)
SGP	Southern Great Plains, Oklahoma			aircraft-pfp	NOAA	(McKain, 2024)
STR	Sutro Tower, San Francisco, California	37.76	−122.45	surface-pfp	NOAA, LBNL	(Schuldt et al., 2021) 8/23/2025 5:26:00 PM

TGC	Offshore Corpus Christi, Texas			aircraft-pfp	NOAA	(McKain, 2024)
THD	Trinidad Head, California			aircraft-pfp	NOAA	(McKain, 2024)
THD	Trinidad Head, California	41.05	−124.15	surface-flask	NOAA	(Lan et al., 2024)
WBI	West Branch, Iowa			aircraft-pfp	NOAA	(McKain, 2024)
WBI	West Branch, Iowa	41.72	−91.35	surface-pfp	NOAA	(Schuldt et al., 2021) 8/23/2025 5:26:00 PM

References

Andrews, A., Crotwell, A., Crotwell, M., Handley, P., Higgs, J., Kofler, J., Lan, X., Legard, T., Madronich, M., McKain, K., Miller, J., Moglia, E., Mund, J., Neff, D., Newberger, T., Petron, G., Turnbull, J., Vimont, I., Wolter, S., Laboratory, N.G.M., 2023. NOAA Global Greenhouse Gas Reference Network Flask-Air PFP Sample Measurements of CH4 at Tall Tower and other Continental Sites, 2005-Present [Data set]. NOAA Global Monitoring Laboratory. https://doi.org/10.15138/35JE-6D55; Date accessed 2024-11-28

Andrews, A., Kofler, J., Trudeau, M.E., Bakwin, P.S., Fisher, M.L., Sweeney, C., Desai, A.R., ESRL, N., 2017. Earth System Research Laboratory Carbon Cycle and Greenhouse Gases Group Continuous Measurements of CO2, CO, and CH4 from Tall Towers, 1992-Present, Version 1.

Andrews A., N. Miles, J. Kofler, M.E. Trudeau, P.S. Bakwin, M.L. Fischer, C. Sweeney, A.R. Desai, B. J. Viner, M. J. Parker, D. A. Jaffe, C. E. Miller, S. F. J. de Wekker, J. B. Miller, K. Thoning, P. Handley, Morris, S., 2024. Continuous measurements of CO2, CO, CH4 on tall towers starting in 1992. NOAA Global Monitoring Laboratory. https://doi.org/10.7289/V57W69F2; Date accessed 2024-11-28

Andrews, A.E., Kofler, J.D., Trudeau, M.E., Williams, J.C., Neff, D.H., Masarie, K.A., Chao, D.Y., Kitzis, D.R., Novelli, P.C., Zhao, C.L., Dlugokencky, E.J., Lang, P.M., Crotwell, M.J., Fischer, M.L., Parker, M.J., Lee, J.T., Baumann, D.D., Desai, A.R., Stanier, C.O., De Wekker, S.F.J., Wolfe, D.E., Munger, J.W., Tans, P.P., 2014. CO2, CO, and CH4 measurements from tall towers in the NOAA Earth System Research Laboratory's Global Greenhouse Gas Reference Network: instrumentation, uncertainty analysis, and recommendations for future high-accuracy greenhouse gas monitoring efforts. Atmospheric Measurement Techniques 7, 647–687. https://doi.org/10.5194/amt-7-647-2014

Aoki, S., Nakazawa, T., Murayama, S., Kawaguchi, S., 1992. Measurements of atmospheric methane at the Japanese Antarctic Station, Syowa. Tellus B 44, 273–281. https://doi.org/10.1034/j.1600-0889.1992.t01-3-00005.x

Blanc, P.-E., Delmotte, M., Lopez, M., Ramonet, M., Xueref-Remy, I., 2025. Atmospheric CH4 product from Observatoire de Haute Provence (100.0 m), 2014-07-16–2025-03-31.

Colomb, A., Ramonet, M., Yver-Kwok, C., Delmotte, M., Lopez, M., Pichon, J.-M., 2025. ICOS ATC NRT CH4 data csv time series from Puy de Dôme (10.0 m), 2025-08-17.

Cristofanelli, P., Trisolino, P., 2020. ICOS ATC CH4 Release from Monte Cimone (8.0 m), 2018-05-03–2020-05-31.

De Mazière, M., Sha, M.K., Ramonet, M., 2025. ICOS ATC NRT CH4 data csv time series from La Réunion (6.0 m), 2025-08-17.

Delmotte, M., Lopez, D., Lopez, M., Philippon, C., Ramonet, M., 2025a. Atmospheric CH4 product from Ersa (40.0 m), 2013-04-25–2025-03-31.

Delmotte, M., Lopez, M., Ramonet, M., 2025b. Atmospheric CH4 product from Finokalia (15.0 m), 2014-06-05–2025-03-31.

Delmotte, M., Ramonet, M., 2025. Atmospheric CH4 product from Ivittuut (2.0 m), 2011-09-01–2014-09-20.
Di Sarra, A.G., Zahn, A., Watson, A., Ankur Desai, Karion, A., Arlyn Andrews, Colomb, A., Scheeren, B., Baier, B., Viner, B., Stephens, B., Daube, B., Labuschagne, C., Myhre, C.L., Miller, C.E., Choong-Hoon Lee, Plass-Duelmer, C., Plass-Duelmer, C., Gerbig, C., Sloop, C.D., Sweeney, C., Kubistin, D., Goto, D., Jaffe, D., Munro, D., Worthy, D., Dlugokencky, E., Kozlova, E., Gloor, E., Cuevas, E., Hintsa, E., Kort, E., Obersteiner, F., Moore, F., Vitkova, G., Manca, G., Brailsford, G., Santoni, G., Haeyoung Lee, Boenisch, H., Timas, H., Matsueda, H., Kang, H.-Y., Huilin Chen, Lehner, I., Mammarella, I., Elkins, J.W., Pittman, J., Pichon, J.M., Müller-Williams, J., Jgor Arduini, Turnbull, J., Miller, J.B., Lee, J., DiGangi, J.P., Hatakka, J., Worsey, J., Holst, J., Kominkova, K., McKain, K., Saito, K., Davis, K., Tørseth, K., Haszpra, L., Gatti, L.V., Emmenegger, L., Sha, M.K., Delmotte, M., Fischer, M.L., Schumacher, M., Torn, M., Leuenberger, M., Heimann, M., Steinbacher, M., De Mazière, M., Lindauer, M., Mölder, M., Martin, M.Y., Ko, M.-Y., Heliasz, M., Marek, M.V., Ramonet, M., Lopez, M., Sasakawa, M., Miles, N., Laurent, O., Hermanssen, O., Trisolino, P., Cristofanelli, P., Krummel, P., Shepson, P., Smith, P., Rivas, P.P., Bergamaschi, P., Keronen, P., Langenfelds, R., Leppert, R., Piacentino, S., Richardson, S., Biraud, S.C., Conil, S., Morimoto, S., Aoki, S., O'Doherty, S., Wofsy, S., Nichol, S., Schuck, T., Lauvaux, T., Seifert, T., Biermann, T., Gehrlein, T., Machida, T., Laurila, T., Aalto, T., Kazan, V., Ivakhov, V., Joubert, W., Niwa, Y., Loh, Z., 2021. Multi-laboratory compilation of atmospheric carbon dioxide data for the period 1983-2020; obspack_ch4_1_GLOBALVIEWplus_v4.0_2021-10-14.
Dlugokencky, E.J., Steele, L.P., Lang, P.M., Masarie, K.A., 1995. Atmospheric methane at Mauna Loa and Barrow observatories: Presentation and analysis of in situ measurements. Journal of Geophysical Research: Atmospheres 100, 23103–23113. https://doi.org/10.1029/95JD02460
Emmenegger, L., Harris, E., Steinbacher, M., 2025. ICOS ATC NRT CH4 data csv time series from Jungfraujoch (13.9 m), 2025-08-17.
Etheridge, D., Langenfelds, P., Guerette, E.A., Thornton, D.P., Krummel, P.B., Loh, Z.M., 2021. CSIRO GASLAB Flask Air Samples, Ver. 3,. Australian Antarctic Data Centre. https://doi.org/doi:10.26179/4gj2-1h44
Gomez-Pelaez, A.J., Ramos, R., Perez-delaPuerta, J., 2006. Methane and carbon dioxide continuous measurements at Izana GAW station (Spain). In: GAW Report (No. 168) of the 13th WMO/IAEA Meeting of Experts on Carbon Dioxide and Related Tracer Measurement Techniques (ed. J. B. Miller). World Meteorological Organization, (TD No. 1359), Boulder, Colorado, USA, 19-22 September 2005 180-184.
Hatakka, J., 2025. ICOS ATC NRT CH4 data csv time series from Pallas (12.0 m), 2025-08-16.
Hatakka, J., Laurila, T., 2025. ICOS ATC NRT CH4 data csv time series from Utö - Baltic sea (57.0 m), 2025-08-12.
Heliasz, M., Biermann, T., 2025. ICOS ATC NRT CH4 data csv time series from Hyltemossa (150.0 m), 2025-08-17.
ICOS RI, 2021. ICOS Atmosphere Release 2021-1 of Level 2 Greenhouse Gas Mole Fractions of CO2, CH4, N2O, CO, meteorology and 14CO2. https://doi.org/10.18160/WJY7-5D06
Kozlova, T., E.;. Heimann, M.;. Worsey, J.;. Leppert, R.;. Seifert, 2020. Cape Verde Atmospheric Observatory: High-precision long-term atmospheric measurements of greenhouse gases (CO, CO2, N2O and CH4) using Off-Axis Integrated-Cavity Output Spectroscopy (OA-ICOS).
Kubistin, D., Plaß-Dülmer, C., Kneuer, T., Lindauer, M., Müller-Williams, J., Zwerschke, E., 2025a. ICOS ATC NRT CH4 data csv time series from Gartow (341.0 m), 2025-08-17.
Kubistin, D., Plaß-Dülmer, C., Kneuer, T., Lindauer, M., Müller-Williams, J., Zwerschke, E., 2025b. ICOS ATC NRT CO2 data csv time series from Hohenpeissenberg (131.0 m), 2025-08-17.
Kubistin, D., Plaß-Dülmer, C., Kneuer, T., Lindauer, M., Müller-Williams, J., Zwerschke, E., 2025c. ICOS ATC NRT CH4 data csv time series from Karlsruhe (200.0 m), 2025-08-17.

Kubistin, D., Plaß-Dülmer, C., Kneuer, T., Lindauer, M., Müller-Williams, J., Zwerschke, E., 2025d. ICOS ATC NRT CH4 data csv time series from Lindenberg (98.0 m), 2025-08-17.
Kubistin, D., Plaß-Dülmer, C., Kneuer, T., Lindauer, M., Müller-Williams, J., Zwerschke, E., 2025e. ICOS ATC NRT CH4 data csv time series from Ochsenkopf (163.0 m), 2025-08-17.
Kubistin, D., Plaß-Dülmer, C., Kneuer, T., Lindauer, M., Müller-Williams, J., Zwerschke, E., 2025f. ICOS ATC NRT CH4 data csv time series from Torfhaus (147.0 m), 2025-08-17.
L. Myhre, C., Platt, S.M., Hermansen, O., Lunder, C., 2021. ICOS ATC CO Release from Zeppelin (15.0 m), 2017-07-27–2021-01-31.
Lan, X., Mund, J.W., Crotwell, A.M., Thoning, K.W., Moglia, E., Madronich, M., Baugh, K., Petron, G., Crotwell, M.J., Neff, D., Wolter, S., Mefford, T., DeVogel, S., 2024. Atmospheric Methane Dry Air Mole Fractions from the NOAA GML Carbon Cycle Cooperative Global Air Sampling Network, starting in 1983, Version: 2024-07-31,. https://doi.org/10.15138/VNCZ-M766
Larmanou, E., Marklund, P., 2025. ICOS ATC NRT CH_4 data csv time series from Svartberget (150.0 m), 2025-08-17.
Lehner, I., 2025. ICOS ATC NRT CH4 data csv time series from Norunda (100.0 m), 2025-08-17.
Lopez, M., Ramonet, M., 2024. Atmospheric CH4 product from Biscarrosse (47.0 m), 2009-09-01–2024-03-31.
Lowe, D.C., Brenninkmeijer, C.A.M., Tyler, S.C., Dlugkencky, E.J., 1991. Determination of the isotopic composition of atmospheric methane and its application in the Antarctic. Journal of Geophysical Research: Atmospheres 96, 15455–15467. https://doi.org/10.1029/91JD01119
Machida, T., Matsueda, H., Sawa, Y., Nakagawa, Y., Hirotani, K., Kondo, N., Goto, K., Nakazawa, T., Ishikawa, K., Ogawa, T., 2008. Worldwide Measurements of Atmospheric CO2 and Other Trace Gas Species Using Commercial Airlines. Journal of Atmospheric and Oceanic Technology 25, 1744–1754. https://doi.org/10.1175/2008JTECHA1082.1
Mammarella, I., 2025. ICOS ATC NRT CH4 data csv time series from Hyytiälä (125.0 m), 2025-08-17.
Marek, M.V., Vítková, G., Komínková, K., 2025. ICOS ATC NRT CH4 data csv time series from Křešín u Pacova (250.0 m), 2025-08-17.
McKain, & N.G.M.Laboratory., K.,. Sweeney, C.,. Baier, B.,. Crotwell, A.,. Crotwell, M.,. Handley, P.,. Higgs, J.,. Legard, T.,. Madronich, M.,. Miller, J.B.,. Moglia, E.,. Mund, J.,. Newberger, T.,. Wolter, S., 2024. NOAA Global Greenhouse Gas Reference Network Flask-Air PFP Sample Measurements of CO2, CH4, CO, N2O, H2, SF6 and isotopic ratios collected from aircraft vertical profiles [Data set]. Version: 2024-08-12. https://doi.org/10.15138/39HR-9N34
Ramonet, M., Conil, S., Delmotte, M., Laurent, O., Lopez, M., 2025a. ICOS ATC NRT CH4 data csv time series from Observatoire pérenne de l'environnement (120.0 m), 2025-08-17.
Ramonet, M., Lopez, M., Delmotte, M., 2025b. ICOS ATC NRT CH4 data csv time series from Trainou (180.0 m), 2025-08-17.
Schuldt, K.N., Tuula, A., Arlyn, A., Shuji, A., Jgor, A., Bianca, B., Peter, B., Tobias, B., Sebastien C., B., Harald, B., Gordon, B., Huilin, C., Aurelie, C., Sébastien, C., Paolo, C., Emilio, C., Bruce, D., Kenneth, D., Martine, D.M., Marc, D., Ankur, D., Joshua P., D., Ed, D., James W., E., Lukas, E., Marc L., F., Luciana V., G., Torsten, G., Christoph, G., Emanuel, G., Daisuke, G., László, H., Juha, H., Martin, H., Michal, H., Ove, H., Eric, H., Jutta, H., Viktor, I., Dan, J., Warren, J., Hui-Yun, K., Anna, K., Victor, K., Petri, K., Mi-Young, K., Katerina, K., Eric, K., Elena, K., Paul, K., Dagmar, K., Casper, L., Ray, L., Olivier, L., Tuomas, L., Thomas, L., John, L., Haeyoung, L., Choong-Hoon, L., Irene, L., Reimo, L., Markus, L., Matthias, L., Zoe, L., Morgan, L., Toshinobu, M., Ivan, M., Giovanni, M., Michal V., M., Melissa Y., M., Hidekazu, M., Kathryn, M., Natasha, M., Charles E., M., John B., M., Fred, M., Shinji, M., David, M., Cathrine L., M., Meelis, M., Jennifer, M.-W., Sylvia, N., Yosuke, N., Simon, O., Florian, O., Salvatore, P., Jean M., P., Jasna, P., Christian, P.-D., Michel, R., Scott, R., Pedro P., R., Kazuyuki, S., Greg, S., Motoki, S., Bert, S., Tanja, S., Marcus, S.,

Thomas, S., Mahesh K., S., Paul, Shepson, Christopher D., S., Paul, Smith, Martin, S., Britton, S., Colm, S., Helder, T., Margaret, T., Pamela, T., Jocelyn, T., Kjetil, T., Brian, V., Gabriela, V., Andrew, W., Steve, W., Justin, W., Doug, W., Andreas, Z., Alcide G., di S., 2021. Multi-laboratory compilation of atmospheric methane data for the period 1983-2020; obspack_ch4_1_GLOBALVIEWplus_v4.0_2021-10-14. https://doi.org/10.25925/20211001

Stanley, K., Pitt, J., O'Doherty, S., 2025. ICOS ATC NRT CH4 data csv time series from Ridge Hill (90.0 m), 2025-08-17.

Sweeney, C., Karion, A., Wolter, S., Newberger, T., Guenther, D., Higgs, J.A., Andrews, A.E., Lang, P.M., Neff, D., Dlugokencky, E., Miller, J.B., Montzka, S.A., Miller, B.R., Masarie, K.A., Biraud, S.C., Novelli, P.C., Crotwell, M., Crotwell, A.M., Thoning, K., Tans, P.P., 2015. Seasonal climatology of CO2 across North America from aircraft measurements in the NOAA/ESRL Global Greenhouse Gas Reference Network. Journal of Geophysical Research: Atmospheres 120, 5155–5190. https://doi.org/10.1002/2014JD022591

Sweeney, C., Miller, J.B., Karion, A., Dinardo, S.J., Miller, C.E., 2016. CARVE: L2 Atmospheric Gas Concentrations, Airborne Flasks, Alaska, 2012-2015. ORNL Distributed Active Archive Center. https://doi.org/i

Tiemoko, T.D., Ramonet, M., Yoroba, F., Kouassi, K.B., Kouadio, K., Kazan, V., Kaiser, C., Truong, F., Vuillemin, C., Delmotte, M., Wastine, B., Ciais, P., 2021. Analysis of the temporal variability of CO2, CH4 and CO concentrations at Lamto, West Africa. Tellus B: Chemical and Physical Meteorology. https://doi.org/10.1080/16000889.2020.1863707

Tohjima, Y., Machida, T., Utiyama, M., Katsumoto, M., Fujinuma, Y., Maksyutov, S., 2002. Analysis and presentation of in situ atmospheric methane measurements from Cape Ochi-ishi and Hateruma Island. Journal of Geophysical Research-Atmospheres 107. https://doi.org/10.1029/2001jd001003

Tsutsumi, Y., Mori, K., Ikegami, M., Tashiro, T., Tsuboi, K., 2006. Long-term trends of greenhouse gases in regional and background events observed during 1998–2004 at Yonagunijima located to the east of the Asian continent. Atmospheric Environment 40, 5868–5879. https://doi.org/10.1016/j.atmosenv.2006.04.036

Worthy, D.E.J., A. Platt, R. Kessler, M. Ernst, Racki, S., 2003. The greenhouse gases measurement program, measurement procedures and data quality, in Canadian Baseline Program; Summary of Progress to 2002. Meteorological Service of Canada.